Three-dimensional microstructure simulation model of cement based materials

Guang Ye[1], Klaas van Breugel[2]

[1] Magnel laboratory for concrete research, Department of Structural Engineering, Ghent University, Belgium

[2] Microlab, Faculty of Civil Engineering and Geosciences, Delft University of Technology, the Netherlands

This paper describes a computer-based numerical model for the simulation of the development of microstructure during cement hydration. Special emphasis is on the algorithm for characterizing the pores. This includes the porosity and the pore size distribution and the topological properties of the porous network. In order to do so, a serial sectioning algorithm and an overlap criterion were employed for the determination of the microstructure. The algorithm for calculating the pore size distribution was also developed. The thus obtained information about the microstructure during cement hydration was further checked against experiments.

Keywords: microstructure, porosity, percolation, modeling, cement-based materials

1 Introduction

Research has shown that quantitative characterization of the cement-paste microstructure based on experiments is not easy. The methodologies, techniques and procedures of the experiments contain numerous uncertainties. First-order geometric parameters of the microstructure of cement paste, such as volume fraction and specific surface area, can be obtained using well-known techniques, e.g. MIP and nitrogen sorption. However, these techniques cannot detect higher order geometrical properties, such as the topology or coordination of the pore network. In particular, with the present experimental techniques it is not possible to obtain the connectivity of the pores, which is a crucial parameter for transport properties, with reasonable accuracy.

Next to experiments, in recent years significant advances have been made in materials characterization and representation by numerical modelling. With the rapid development of computer technology, a number of experimental complications may be circumvented, or at least reduced, by using computer-based simulation models. With these models it is possible to simulate the evolution of the microstructure, especially the pore structure, in hardening cementitious materials. However, computerization brings to the forefront a new problem, i.e. how to draw correctly the geometrical

3.1 *Direct representation of three-dimensional pore structures*

The serial sectioning method starts with scanning the simulated 3D microstructure from three orthogonal directions, layer by layer. Figure 3, bottom left and bottom right, shows the solid phase sections and pore phase sections, respectively.

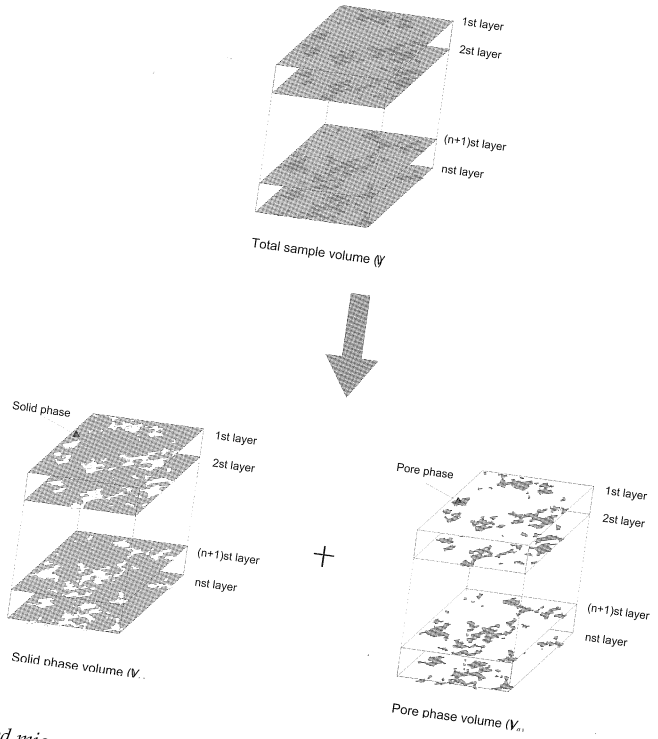

Figure 3. Simulated microstructure considered as serial sections. Solid phase (left) and porous phase (right).

Consider a 3D sample that occupies a set $\alpha \subset R^n$ of the physical space (n=2 in two dimension and n=3 in three dimensions). The serial sectioning method starts with scanning the sample layer by layer. An arbitrary point p belongs either to the subset of the solid phase S or to the subset of the capillary pore phase L in each layer. Thus, the sample α contains two disjoined subsets:

$$\Omega = S \cup L \tag{1}$$

$$S \cap L = 0 \tag{2}$$

where 0 is the empty set. Furthermore, the overlap algorithm checks each one of the six faces of this spatial point on its upper layer and lower layer and examines whether this point is connected with its neighbors of the same phase. This procedure is repeated until the final layer of the body. Therefore, two new subsets of the connected solid phase S' ($S' \subset S$) and the connected capillary

pore phase L' ($L' \alpha L$) are found. $T_{(S)}$ and $T_{(L)}$ give the volume fractions of the total solid phase and the total capillary pore phase.

$$T_{(S)} = V_{(S)}/V_{(P)} \tag{3}$$
$$T_{(L)} = V_{(L)}/V_{(P)} \tag{4}$$

where $V_{(S)}$, $V_{(L)}$ and $V_{(P)}$ denote the volume of solid phase, capillary pore phase and total sample, respectively.
The ratios $C_{(S)}$ and $C_{(L)}$ represent the connected volume fraction of the solid phase and of the capillary pore phase:

$$C_{(S)} = V_{(S')}/V_{(P)} \tag{5}$$
$$C_{(L)} = V_{(L')}/V_{(P)} \tag{6}$$

where $V_{(S')}$ and $V_{(L')}$ denote the connected solid phase volume and the connected capillary pore volume.
The hydraulic radius is a useful measure of the "size" of the pore in the case of irregularly shaped cross sections [9]. According to the definition given by Dullien [4], the hydraulic radius R_H can be computed as

$$R_H = A/P \tag{7}$$

where A is the cross sectional area of a pore and P is its perimeter.
The coordinates of the gravity center of each pore can be approximately computed by

$$X = sum(x)/count \tag{8}$$
$$Y = sum(y)/count \tag{9}$$

where X and Y are the coordinates of the gravity center for a pore in a certain layer Z, $sum(x)$ and $sum(y)$ are the summation of the x coordinates and the y coordinates of each pixel belonging to the pore and *count* is the number of pixels in the pore.
Thus, each individual pore with its 2D features, including perimeter, area and gravity center coordinates, is stored and ready for the determination of interconnectedness of the pores.

3.2 Algorithm implementation

The procedure for characterizing the features of each 2D section starts from checking neighboring pixels with the aid of an array that contains the coordinates of neighboring pixels relative to the pixel currently analyzed. The advantage is that the check can be done with a simple one-dimensional array. In the next layer, every pixel is checked once again to determine if a pixel is part of a pore and to number the pores accordingly. Whenever an edge is found, a new pore is created and given a new number. Further, a recursive function for calculating the perimeter is called. By tracing the edge and marking each edge pixel, the length of the perimeter is obtained. If the program finds

another edge pixel that belongs to a pore that already has a number, it means that this pore is a part of the same pore and therefore the pore number is changed to the number of that particular pore. The perimeter and the pore number are saved. Another recursive function for calculating the area is called, which will calculate not only the edge pixels, but also all pore (or solid) pixels to count their area. When the pore is not connected to any other pore, it is given a new pore number, higher than the last pore number that was recorded. The pore data is then connected to the general list of pores, to the appropriate branch according to its pore number and the layer where it was found. When a new pore with the same pore number and the same layer is found, the object is discarded, but the area and perimeter information is added to the existing data for the particular pore.

3.3 Topology of pore structure

Connectivity and Genus

The topological parameters, characterizing the interconnectedness of "shape" or "structures", are the "connectivity" and the "genus" [4]. Connectivity is a measure of the alternative (multiply connected) paths, which are available to fluid flow, diffusion, etc., in porous media. It is defined as the number of nonredundant closed-loop paths by which all regions inside the shape can be inspected (see Figure 4). Redundant loops are those that may be transformed into another by deformation, that may be shrunk into a point without passing out of the closed surface, or that do not give access to any new part of the shape. A basic theorem of topology states that the "connectivity" of a closed surface or shape is equal to its "genus" G. Genus is the largest number of cuts that may be made through parts of the shape without totally disconnecting any part from the rest [4]. Following the same principle, Lymberopoulos & Payatakes [8] defined the "genus" number as the maximum number of non-intersecting closed curves that can be made upon the surface of a structure without separating it into disconnected parts. It is equal to the number of distinct holes through a structure, or to the maximum number of cuts that a multipleconnected structure can undergo in order to form a simply connected one.

A general theorem of topology states [4]:

$$G = b - n + N \tag{10}$$

where b is the number of branches, n is the number of nodes and N is the number of separate networks.

A typical example (Figure 4) of doughnut gives a good explanation of the "connectivity" and "genus". The doughnut in Figure 4a has genus 1 because its whole exterior can be explored through 1 closed-loop path and no more than 1 cut can be made without the part being disconnected. Twisting or stretching the doughnut would not change the topology. In Figure 4b the appendix attached to the doughnut does not change the topology. The shape in Figure 4c has genus 2 because there are 2 non-redundant loops; the third one shown as dotted line is redundant. Figure 4d shows an example of genus 3.

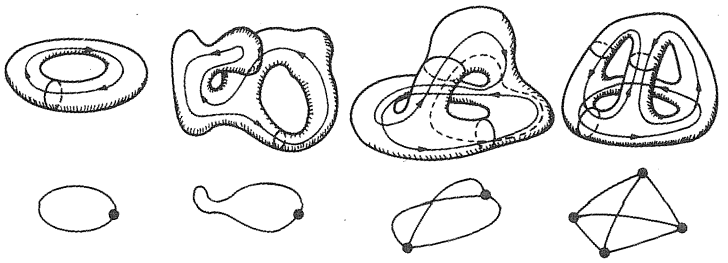

Figure 4. Illustration of the concepts of "connectivity" and "genus" After [4].

Connectivity determined with the serial section method

The connectivity of a porous material can be determined with a serial section method. To do so, the overlap criterion has to be applied.

Overlap criterion: The overlap between two 2D features exists if the features belong to adjacent layers, and at least one perpendicular line exists on which both features have the same phase.

The determination of the interconnectedness between the features on the serial sections is achieved with the linked-list network structure shown in Figure 5. An example of analyzed pore structure is shown in Figure 6.

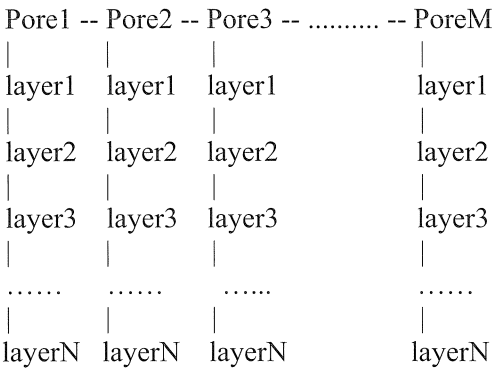

Figure 5. Linked-list network structure for determination of the interconnectedness on serial sections.

In this linked-list structure, each pore is a 3D-pore set and each pore in the branch consists of objects from 3D pore structure data. A cumulative function automatically puts the data in their right place according to a pore ID number and their layer number. Next, the current pore ID is

compared with the upper layer number; if the ID number is larger, the new data is a new pore and a new pore is created and added to the end of the list. If this pore ID is smaller than the top layer ID, the program searches for the correct place to keep the number in order and then makes a new node and puts it between existing nodes.

A "move-pores function" is used for multi-layer analysis if two pores, that at first seem to be separated, are found to merge on subsequent layers. Then a new node is recorded and all the data need to be removed. Afterwards, all the nodes from one linked-list structure are transferred to the appropriate linked-list structure object and the empty branch is discarded.

A modified formula by Lymberopoulos and Payatakes [8] for computing the topological parameter genus *G* was applied:

$$G_{min} = b_{in} - n_{pore} + N_{in} \tag{11}$$

$$G_{max} = (b_{in} + n_{out}) - (n_{pore}+1) + [(N_{in} - N_{out}) + 1] \tag{12}$$

where b_{in} is the number of connections between overlapping features of pores or solid, b_{out} is the number of pore channels intersected by the sample boundaries, n_{pore} is the number of pores, N_{in} is the overall number of separate networks, and N_{out} is the number of separate networks which have access to the boundaries of the sample.

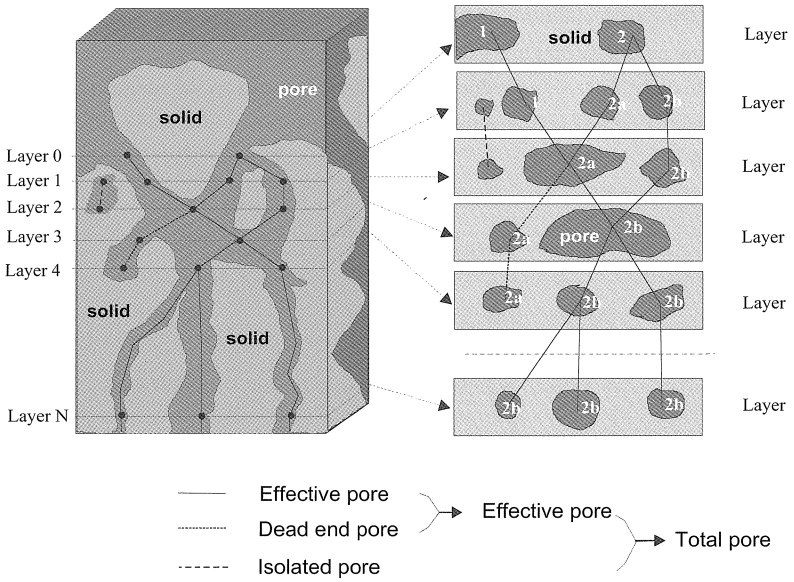

Figure 6. Pore network structure determined by overlapping criterion. Distinction between effective pores, dead-end pores and isolated pores.

For example as shown in Figure 6, pore 1 and pore 2 are already in layer 0. During scanning of layer 1, three pores are found. One of them is found to overlap with pore 1 and the other two are overlapping with pore 2. However, since these three pores are not connected in this layer, the pore

ID 1 and 2 are assigned. Subsequently, if one finds that pore 1 is connected with pore 2 in layer 2; a node is found and the data of pore 1 detached from the main list. A new ID (2) is assigned and then added again to the list, as a part of the pore-2 branch. After the analysis outlined above, the number of connections between overlapping features b_{in} is 15, the number of pore channels intersected by the sample boundaries b_{out} is 3, the number of pores n is 15, the overall number of separate networks N_{in} is 1 and N_{out} is 1. According to Eq. 11 and Eq. 12, the calculated genus number G_{min} is 1 and G_{max} is 3.

Pore size distribution

The algorithms for the determination of the characteristic pore size distribution spectra of a simulated 3D binary image described by Bekri et al. [10], can be employed for our spherical-based 3D pore structure. In principle, the simulated pore structure is the inverse free space between the expanding cement grains. The pore size distribution curve can be determined by considering the sub-volumes of the system that are accessible for spheres of different radii r. Let $\alpha_{(r)}$ be the volume fraction of the pore space "coverable" by spheres of radius r (Figure 7). $\alpha_{(r)}$ is a monotonically decreasing function of r and can easily be compared with the "cumulative pore volume" curves measured by mercury intrusion porosimetry.

$$\phi_{(r)} = \frac{4k\pi}{3}\sum_{r=m}^{n}\left(\frac{r}{2}\right)^3 \tag{13}$$

where m and n are the maximum radius and minimum radius of the sphere which can be "put" into the system, respectively. The minimum radius n is largely depending on the computer capacity. k = 1.83 is a geometrical factor to covert the volume of void from spherical based volume to cubic-based volume.

The derivative $-d\alpha_{(r)}/dr$ is the fraction of volume coverable by pore spheres of radius r but not by spheres of radius $r+dr$ and is a direct definition of the pore size distribution. The $\alpha_{(r)}$ of the pore spheres with radius r can be computed by packing pore spheres in the free space.

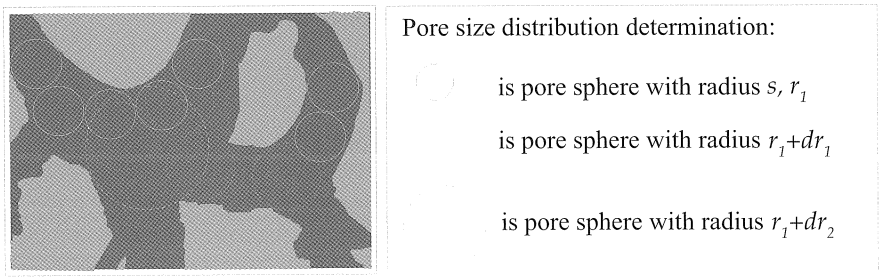

Figure 7. Pore size distribution as determined by calculating pores which could be covered by fictitious spheres of radius r.

4 Results and discussions

4.1 Parameters for simulation

The main variables considered in the simulation are:

- Degree of hydration.
- Water/cement ratio. Samples with w/c ratio of 0.30 to 0.60 with Blaine fineness 420 m^2/kg were simulated.
- Fineness of cement particles. Blaine fineness of cement 210 m^2/kg, 420 m^2/kg and 610 m^2/kg were considered for w/c ratio 0.40.
- Resolution of pixels. For the sample with w/c ratio 0.40 and Blaine fineness of 420 m^2/kg, resolutions 2 μm, 1 μm and 0.25 μm were used.

A continuous particle size distribution, with a minimum particle size 2 μm and maximum size 45 μm, was used for all samples. The size of the sample was 100x100x100 μm^3. Table 1 shows the number of particles in the cubic body involved in the calculation.

Table 1. Initial number of particles in the calculation body of 100 μm^3.

samples		number of particles involved
w/c	Blaine fineness m^2/kg	
0.30	420	8968
0.40	420	8168
0.50	420	6716
0.60	420	5898
0.40	210	3253
0.40	420	8168
0.40	610	12607

4.2 Influence of water/cement ratio

Degree of hydration

The degree of hydration simulated by HYMOSTRUC is shown in Figure 8. The simulated results were compared with the heat release measured by isothermal calorimeter up to 14 days of age. A good agreement between simulations and experiments was found.

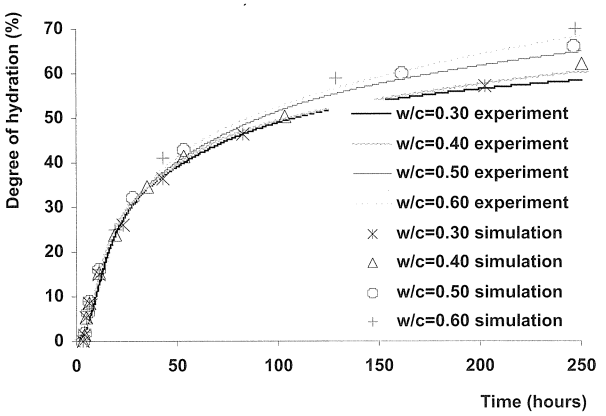

Figure 8. Degree of hydration of cement paste as a function of hydration time.

Visualization of microstructure

The simulated pore structures are visualized in Figure 9 for the samples with w/c ratio 0.30, 0.40, 0.50 and 0.60 at a degree of hydration of 0.75. It is obvious that at the same degree of hydration, the sample with lower w/c ratio shows lower porosity than the samples with a higher w/c . The calculations revealed a capillary porosity of 6%, 19%, 28% and 35% for w/c 0.30, 0.40, 0.50 and 0.60, respectively.

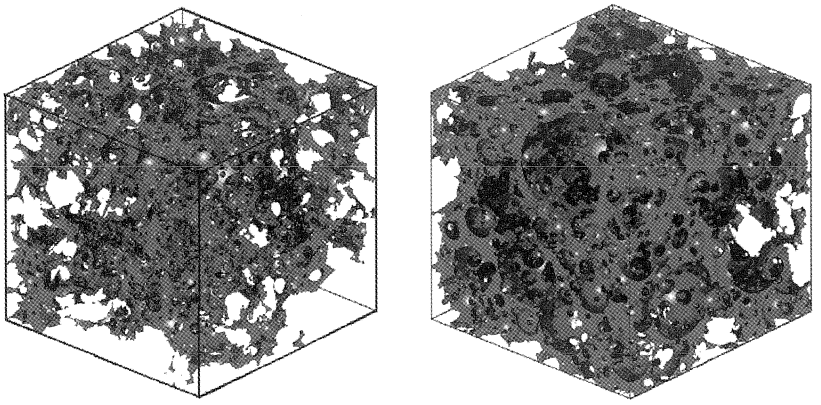

a) w/c= 0.30 *b) w/c = 0.40*

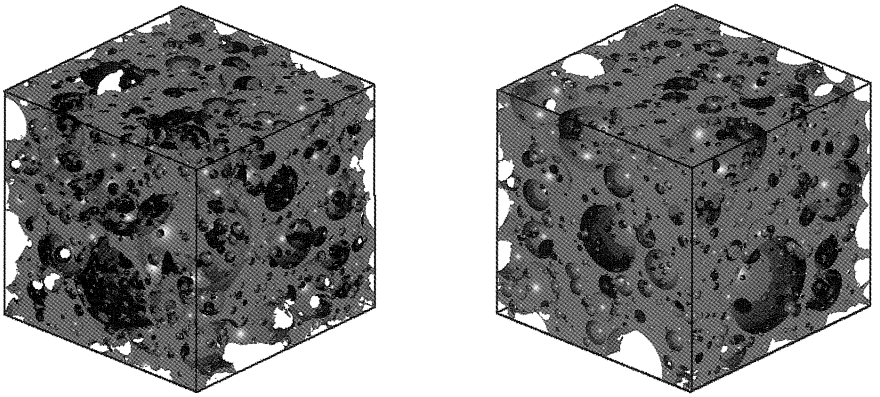

c) w/c = 0.50 d) w/c=0.60

Figure 9. Simulated pore structure at a degree of hydration 0.75 for the samples with: a) w/c ratio 0.30, α_c =6%, b) w/c ratio 0.40, α_c =19% c) w/c ratio 0.50, α_c =28%, and d) w/c ratio 0.60, α_c =37%.

Microstructural parameters

For each sample, the internal surface area, the hydraulic radius, the total porosity and the connectivity of the porosity were calculated at different hydration stages as shown in the Figures 10 - 12. The characteristic pore size distribution curves are illustrated in Figure 13 at the degree of hydration 0.64.

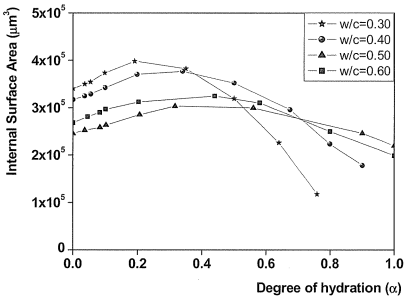

Figure 10. Internal surface areas of capillary pores in cement paste as a function of degree of hydration.

As shown in Figure 10, the samples with the lowest w/c ratio displayed the highest internal pore surface area at early age. However, after a certain degree of hydration, the surface area of the lower w/c ratio samples decreases more rapidly. If we look back to Table 1, the samples with lower w/c ratio have a higher solid fraction, i.e. greater number of cement particles. This implies that, per unit volume of paste, more cement surface is in contact with water. However, in the later stage, since there is less initial water in the lower w/c sample and most of it has reacted and converted into hydration products, only little capillary pores remain. This explains why both the hydraulic radius and capillary porosity decrease with a reduction in w/c ratio and with an increase in the degree of hydration, as shown in Figure 11 and Figure 12. This was also shown by the visualized pore structure illustrated in Figure 9.

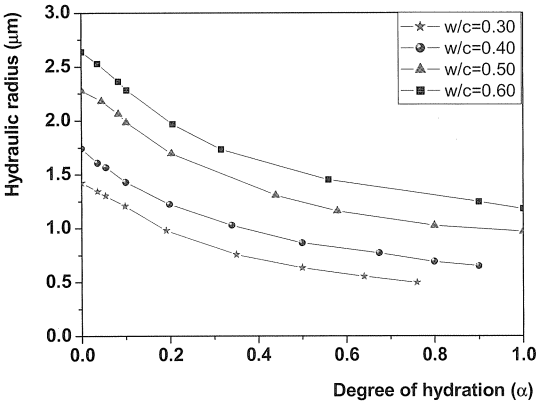

Figure 11. Simulated hydraulic radius in cement paste as a function of degree of hydration.

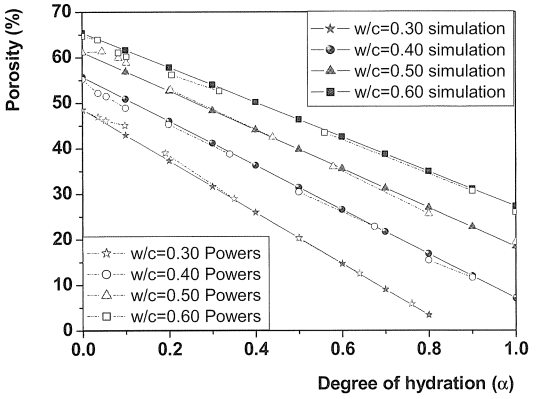

Figure 12. Simulated capillary porosity of cement paste as a function of the degree of hydration compared with Powers' model.

The hydraulic radius obtained in the present simulation decreases from 1.15 mm to 0.60 μm for a cement paste with w/c 0.40 with a degree of hydration increasing from 0.3 to 0.9. The present results are two orders of magnitude higher than experimental result obtained by Jiang et al. [11]. The total porosity compared with Powers' model [12] as a function of the degree of hydration for different w/c ratio, is plotted in Figure 12. The simulation results agree very well with Powers' model.

The simulated pore size distribution curve is plotted in Figure 13 for the samples with w/c 0.30 and 0.60 at a degree of hydration 0.64. The sample with higher w/c ratio displays a peak around 5 μm and the sample with lower w/c ratio exhibits a peak around 0.9 ~2 μm.

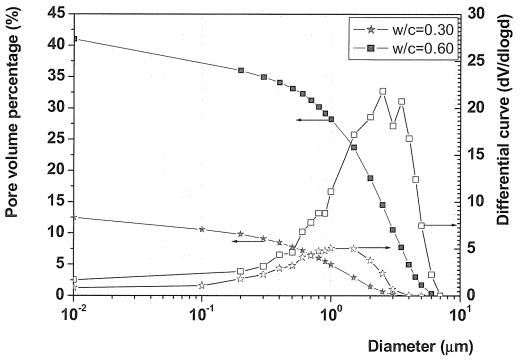

Figure 13. Simulated pore size distribution of cement pastes with w/c ratio 0.30 and 0.60 at a degree of hydration 0.64 (Blaine fineness of cement 420 m^2/kg).

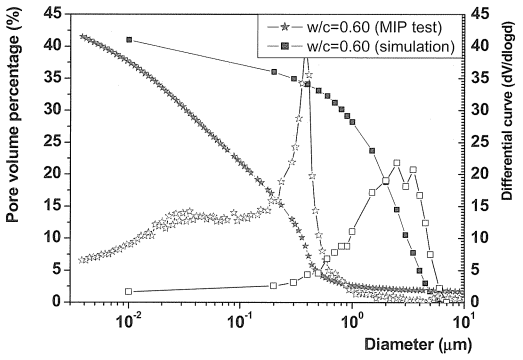

Figure 14. Simulated pore size distribution compared with MIP test for the sample with w/c 0.60 at a degree of hydration 0.64.

The simulated pore size distribution of the sample with w/c 0.60 at a degree of hydration 0.64 was also compared with the MIP test results [13]. The pore sizes determined by numerical simulation are one order of magnitude higher than those found in the MIP test.
By applying backscatter SEM techniques, shown in the next section, the difference between the simulated pore size distribution and MIP test will be analyzed and discussed. In particular, it will be shown how the inkbottle effect influences the measured pore size distribution.

Percolation of microstructure

The percolation theory deals with disordered multiphase media in which the disorder is characterized by the degree of connectivity of the phases. The microstructure of cement-based materials provides numerous examples of percolation phenomena [14]. In percolation studies one is often interested in the fraction of a phase, which is connected across the microstructure as a function of the total volume fraction of the phase. In particular, the de-percolation of capillary porosity is of great interest for studying the transport phenomena in cement-based materials.

Figure 15 shows results of the percolation threshold of the solid and capillary porosity for two different w/c ratios. The solid percolation threshold was found at a degree of hydration 0.02 for w/c ratio 0.3 and at a degree of hydration 0.025 for w/c ratio 0.4. Afterwards, the connected solid phase shows a quick increase and all solid particles are connected at a degree of hydration of 0.25 for both w/c ratio samples. These findings are in fairly good agreement with ultrasonic pulse velocity (UPV) tests performed on cement pastes with the same w/c ratios [13]. In the experiments, a sudden change of UPV was reported after 3 hours hydration. After 30 hours, the UPV increased only slowly until the end of the experiment. Similar results have also been found in the literature [15-17].

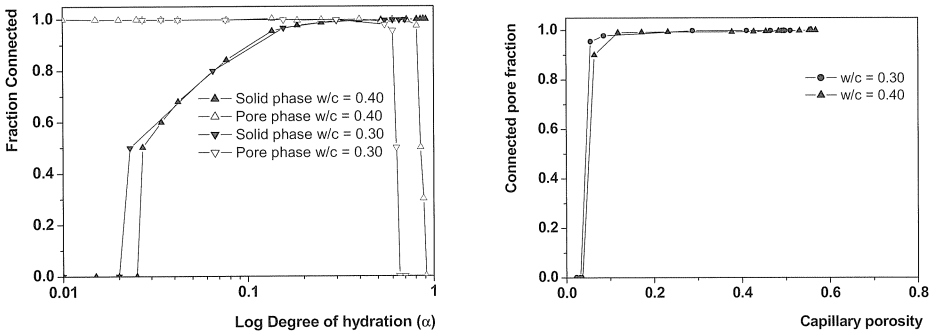

Figure 15. Development of microstructure in cement paste with two different w/c ratios. Left: connected fraction of the phases as a function of degree of hydration. Right: connected pore fraction as a function of capillary porosity.

For the evolution of the capillary porosity, Figure 15 shows that almost all capillary pores are connected with each other up to a degree of hydration of 0.70. A value of 3.5% of the capillary porosity percolation threshold is found in both samples, corresponding to a degree of hydration 0.91 for the sample with w/c ratio 0.4 and a degree of hydration 0.63 for the sample with w/c ratio 0.3. The evidence of a constant value of the capillary porosity percolation threshold is in good agreement with simulations performed with the CEMHYD3D model [18].

Connectivity of capillary pore structure

Calculations of the connectivity were performed for samples with w/c ratios 0.30 and 0.40, at a degree of hydration 0.70. Table 2 includes the most important calculation results. The evolution of the calculated value of the genus/volume versus the sections examined is shown in Figure 16. The upper and lower limits of the genus for the sample with w/c = 0.30 are G_{min} = 448 and G_{max} = 361. For the sample with w/c ratio 0.40 values of G_{min} and G_{max} were 753 and 904, respectively.
It is clear that, at the same degree of hydration, the genus number for the sample with w/c = 0.30 is larger than that of the sample with w/c = 0.40. This means that a more complex fluid channel is formed in the sample with lower w/c, which is to be expected since more pores are connected with each other in the sample with higher w/c ratio.

Table 7.2. Calculation of the connectivity of capillary pore structure.

w/c	degree of hydration [-]	total porosity [%]	connected porosity [%]	connected porosity fraction [%]	average pores number in 2D	average links between 2 layers	G_{min}	G_{max}
0.30	0.70	8.63	8.44	97.8	42.08	40.16	753	904
0.40	0.70	20.45	20.41	99.8	28.45	26.76	361	448

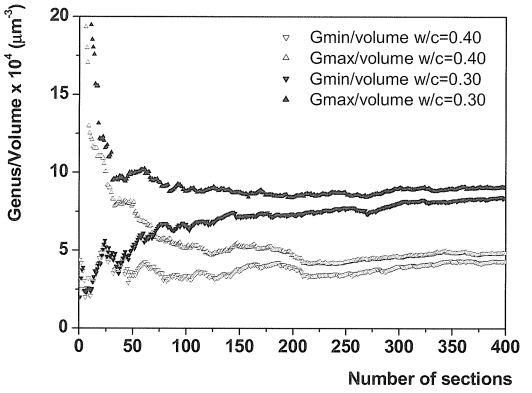

Figure 16. Distribution of the calculated ratio genus/volume versus the number of the sections examined. Samples with w/c = 0.30 and w/c = 0.40 at degree of hydration 0.70.

4.3 Influence of fineness of cement particles on the simulated pore structure

Three Blaine fineness, i.e. 210, 420, and 610 m^2/kg, were used, representing a coarse, normal and a fine cement. In Figure 17 it can be observed that the coarse and fine cement differ significantly from the "normal" cement with a Blaine fineness of 420 m^2/kg. The degree of hydration calculated with the HYMOSTRUC model is presented in Figure 17 for the three different cement finenesses.
With respect to the degree of hydration shown in Figure 17 it is noticed that in practice a degree of hydration close to 100% is generally not reached. In ordinary concrete mixtures the maximum degree of hydration will not be higher than about 70%. In this study, however, the emphasis was on the relationship between degree of hydration and evolution of the pore structure and not on if and how the degree of hydration could have been reached.

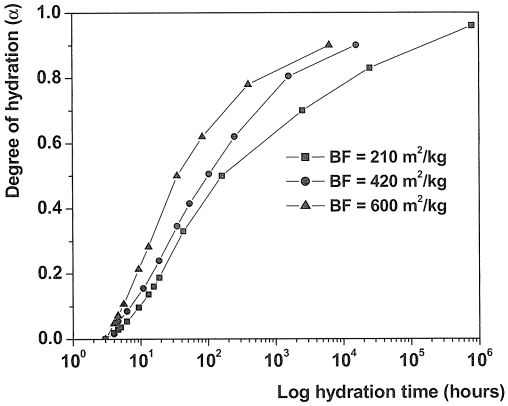

Figure 17. Degree of hydration for the samples with different fineness of the cement at isothermal curing at 20 °C.

Visualization

The simulated pore structures are presented in Figure 18 for the samples with Blaine fineness of 210, 420, and 610 m^2/kg at a porosity of 15%. The calculated minimum genus number was 109, 361 and 562, respectively. This implies that the pore shape for the sample with finer cement particles is more irregular than the sample with coarse cement. This can also be seen from the pore size distribution shown in Figure 20.

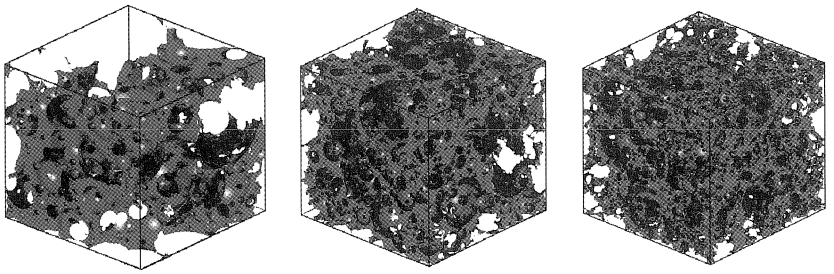

Figure 18. Simulated pore structure for the sample with Blaine value of 210 m^2/kg (left), Blaine value of 420 m^2/kg (middle), Blaine value of 610 m^2/kg (right), at porosity α_c = 15%.

Percolation of microstructure

The influence of the cement fineness on the percolation threshold of the solid phase and of the capillary pore phase, in terms of connected volume of a fraction as function of the degree of hydration (α), is shown in Figure 19.

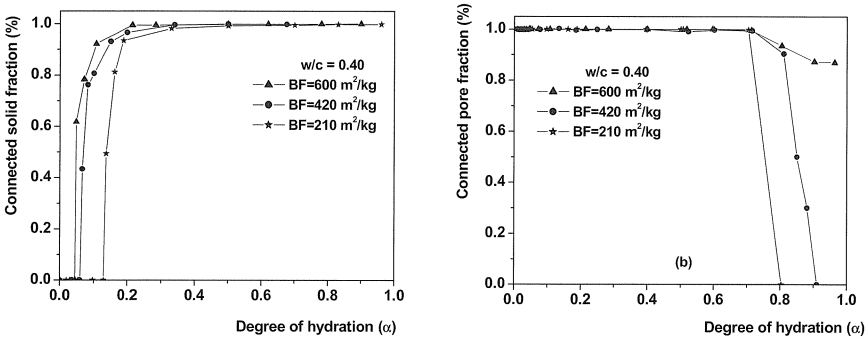

Figure 19. Influence of cement fineness on the percolation of microstructure. Left, solid phase; right, pore phase.

In the Figure 19, left, it can be seen that the finer the cement, the quicker the solid phase percolation threshold will be reached. The percolation threshold occurs at a degree of hydration 0.05 and 0.14 for the samples with Blaine fineness of 610 m^2/kg and 210 m^2/kg, respectively.
In Figure 19, right, it is shown that, according to the numerical model, for the sample with the finest cement the de-percolation threshold of the capillary pores cannot be reached.

Pore size distribution

Figure 20 shows the effect of cement fineness on the pore size distribution. Relatively big pores can be found in the sample with coarser cement. Smaller pores exist in the sample made with finer cement.

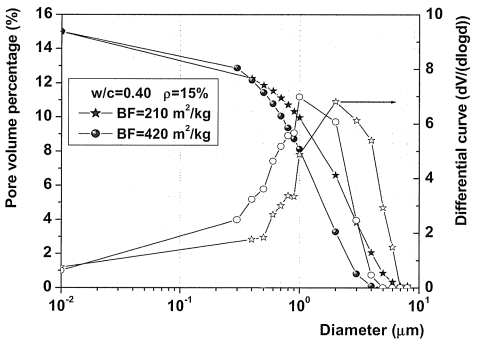

Figure 20. Influence of cement fineness on the pore size distribution presented by the numerical simulation model.

5 Discussion

5.1 Percolation of capillary porosity

The simulation results on the percolation of phases of the microstructure discussed in the previous paragraph will be compared with similar results with the CEMHYD3D model [14] and Navi's model [19].

For a sample with w/c ratio 0.40, Figure 21, shows a comparison of the fraction of connected solid and capillary pore phases simulated with the CEMHYD3D model and with HYMOSTRUC3D. Note that in the CEMHYD3D model only four sizes of particles were used, viz. diameters 3, 9, 13 and 19 pixels were used. The size of sample was 100x100x100 μm^3 and the resolution in this case was 1 µm/pixel [18]. In HYMOSTRUC3D, a continuous particle size distribution, between minimum size 2 mm and maximum size 45 µm was used. The size of the sample was the same as in the CEMHYD3D simulation and the resolution of the images were 0.25 µm and 1 µm.

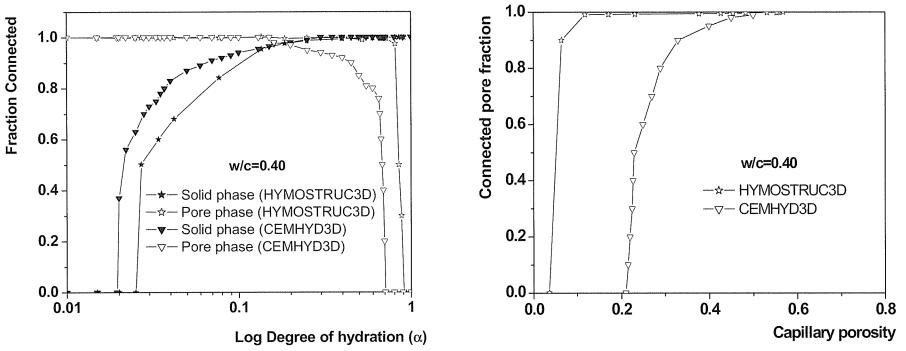

a) Connected volume fraction of solid and pore different degrees of hydration

b) Percolation threshold of the capillary phases at pores

Figure 21. Development of the microstructure simulated by HYMOSTRUC3D and CEMHYD3D (resolution 1µm/pixel).

The development of the connectedness of the solid phases in both models is quite similar. These two models both reach a solid phase percolation threshold at a degree of hydration around 0.02 - 0.03. At a degree of hydration of 0.20 ~0.25, nearly all solid phases, i.e. unhydrated cement core, C-S-H gel and $Ca(OH)_2$, are connected.

However, significant differences in the simulated evolution of the capillary pore structure between the two models are shown in Figure 21b. Firstly, the capillary pore space percolation threshold is found to be about 20 - 22% in the CEMHYD3D model [18], whereas in HYMOSTRUC3D the percolation threshold of the capillary porosity is found at about 3.5%. Secondly, the pore space percolation threshold occurs in the CEMHYD3D simulation at a degree of hydration of 0.70, but in HYMOSTRUC3D the capillary porosity percolation threshold occurs much later, at a degree of hydration around 0.90 (Figure 21a).

Why are the differences in capillary porosity so pronounced in the two models? To answer this

question, the principle of both hydration models must be understood. In the CEMHYD3D model the different cement components are simulated as different sets of digital pixels. For example, when C_3S hydrates, a cellular automaton model is applied in which the reactants (pixels) dissolve from their matrix and walk around in the capillary water space. When two reactants meet at a certain place, a chemical reaction occurs and the reaction products will be located at that place. Consequently, a lot of smaller capillary pores are blocked by these "walking around" hydration products. In other models, such as HYMOSTRUC or Navi's model [19], the cement particles and hydration products are simulated as spheres. The growing spheres are overlapping when cement hydration takes place. The pore space percolation threshold of the spherical-based models has been found always around a few percent porosity [20].

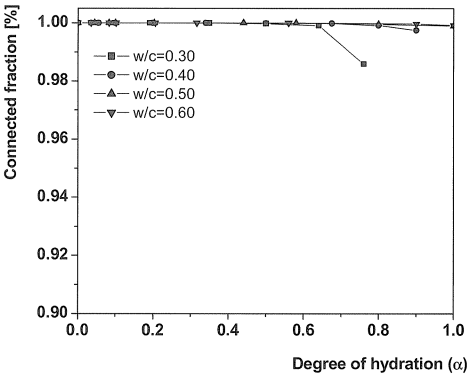

Figure 22. The connectivity of the porosity as function of the degree of hydration (resolution 0.25 μm/pixel).

Another important factor that affects the capillary pore space percolation is the digital resolution. Figure 22 presents the connected porosity fraction as a function of the degree of hydration. The image resolution was 0.25 μm/pixel. It is noticed that for all samples the capillary pores are almost always connected, even at ultimate hydration. These results, that no de-percolation of capillary porosity can be found, are quite different from the result of the CEMHYD3D model [18], but similar to the results previously calculated by Navi et al. [19].

For example, Navi's model [19] showed that the percolation threshold of the capillary pore space changed from 30%, 12% to 0% if the digital resolution increased from 10 μm/pixel, 5 μm/pixel to 2 μm/pixel for a cement paste with w/c 0.40. In the CEMHYD3D pixel-based simulation model [18], the percolation threshold of the capillary porosity changed from 24%, 18% and 11% if the digital resolution shifted from 1 μm to 0.5 μm and 0.25 μm in a cement paste with w/c 0.30. This can be explained because smaller pores can be resolved at the greater resolutions, and the pathways that would seem to be closed at low resolution are seen to be open at higher resolutions. In the present simulation, the digital resolution was 0.25 μm/pixel; at this high digital resolution, even very small capillary pores pathways were detected, leading to a very low percolation threshold of the capillary porosity or no threshold at all.

It can be concluded that the connectivity of the pores is strongly influenced by the digital resolution and also by the layer depth in the image-based calculation. To accurately define the digital resolution, one has to consider the computation time needed and the reliability of the calculation result. If

one uses this simulated pore structure for predicting the transport properties, the accuracy of this simulated pore structure will directly influence the reliability of the calculated water permeability. For validating the predicted percolation threshold of the capillary porosity, permeability experiments have to be carried out, as it was done in [13].

5.2 SEM image and HYMOSTRUC 2D image

This paragraph will give a comparison of the images obtained from SEM experiments and the images simulated with the HYMOSTRUC model. The results of image analysis will show similarities in the 2D pore size distribution of experiments and simulations.

Figure 23 presents the cement paste and its pore structure obtained by BSE. Figure 24 shows the simulated cement paste with the HYMOSTRUC model. Both pastes had a w/c ratio 0.30 and were 14 days old, corresponding to the degree of hydration 0.60.

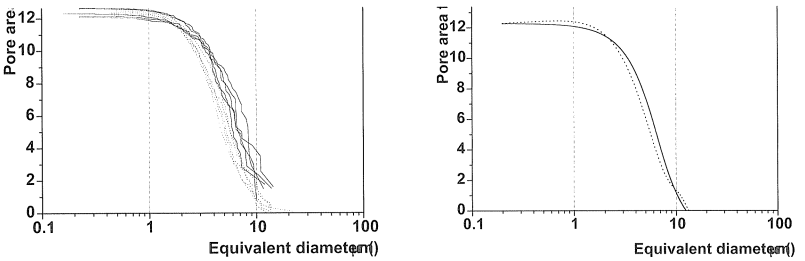

Figure 25 Left: 2D "pore size" distribution of simulated cement paste and ESEM image analysis for the w/c 0.3 cement paste. Right: Regression curves from samples.

Figure 25, left, presents the results from the image analysis and the HYMOSTRUC simulation. The equivalent pore diameter versus the pore area fraction represents the

Figure 23. SEM image of cement paste with w/c ratio 0.30 at age 14 days. Left: Original grey scale image. Right: after segmentation and noise removal. Field size (100x100 μm).

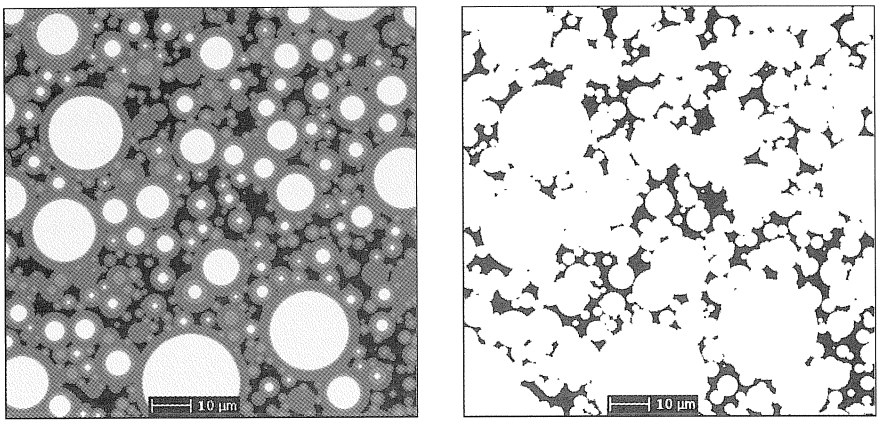

Figure 24. Simulated cement paste with w/c ratio 0.30 at degree of hydration 0.60. Left: from white to black shows unhydrated cement cores, inner products, outer products and capillary pores. Right: capillary pores only. Field size (100x100 μm).

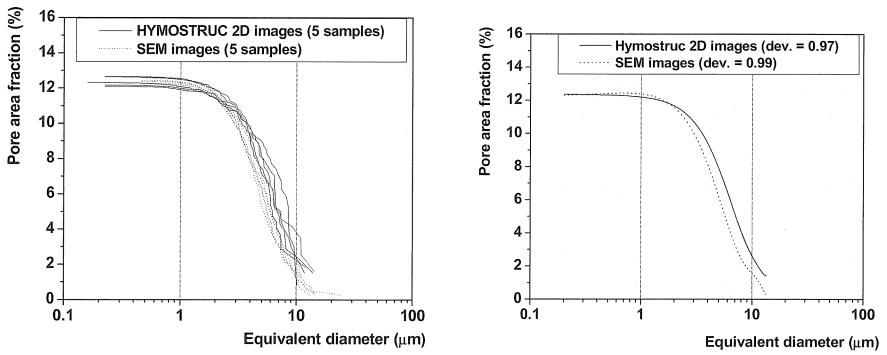

Figure 25. Left: 2D "pore size" distribution of simulated cement paste and ESEM image analysis for the w/c 0.3 cement paste. Right: Regression curves from samples.

Figure 25, left, presents the results from the image analysis and the HYMOSTRUC simulation. The equivalent pore diameter versus the pore area fraction represents the two-dimensional pore size distribution. For 5 samples, taken from arbitrary positions both from the SEM image and the simulations, the regression curves are plotted in Figure 7.28, right. The R-squared value of a simulated 2D image and a SEM image are 0.97 and 0.99, respectively. These figures show that there is good agreement between the simulated pore structure and BSE image analysis. The simulated pores are slightly larger than in the BSE image in the large pore region only. The size of almost all pores is less than 20 μm, both in the experiments and in the simulations.

5.3 Pore size distribution from MIP experiments and HYMOSTRUC simulations

A comparison of the pore size distribution from mercury intrusion porosimeter test and from the simulations with the HYMOSTRUC model will provide a good insight in the difference of the pore structures. This result is also a guide for making a good permeability model.

Figure 26 presents the comparison of pore size distribution by experiment and by simulation for the cement paste with w/c ratio 0.30, 14 days old. The pore size distribution shows a smaller pore volume of pore sizes between 0.03 μm up to 2 μm. This difference might be attributed to the limitations of the MIP test method. As we know, the MIP test method suffers from the "ink bottle" effect, which means that large pores are preceded in the intrusion path of the mercury by smaller necks. This problem produces pore size distribution curves with erroneously high volumes of smaller pores and erroneously small volumes of larger pores [21-23]. In the simulation, however, the pore size distribution curve was determined by calculating the sub-volumes of the pore space that were accessible to testing spheres of different radii *r*. This method avoids the "ink bottle" effect, taking all pores into account in the "right" size.

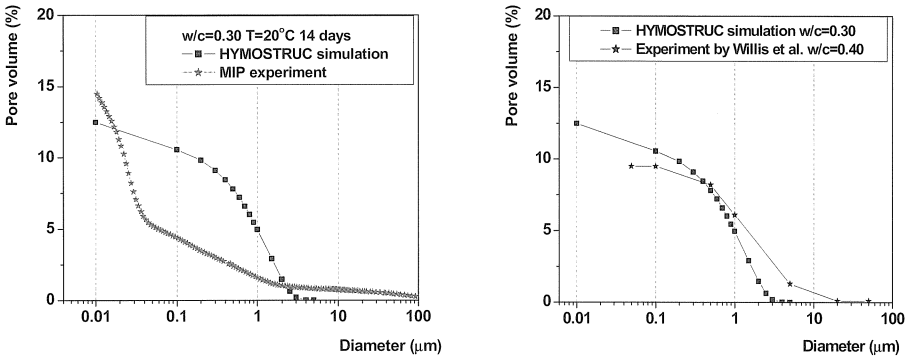

Figure 26. Comparison of pore size distribution by experiment and simulation for a 14-day-old w/c 0.30 cement paste, left. Comparison of simulation and Wood's metal intrusion porosimetry test by Willis et al. (after [23]), right.

Willis et al. [22] extensively investigated the "ink bottle" effect using Wood's metal intrusion porosimetry (WMIP) and image analysis. They concluded that pore size distributions obtained from MIP are shifted towards small pores compared to those obtained from WMIP and image analysis. A comparison between the present simulation and image analysis size distribution of WMIP is shown in Figure 26, right. In their original paper Willis et al. [22] presented their plots as volume vs. pore area at pressure 5000 psi. Diamond [23] recalculated the data as pore volume vs. pore diameter. From Figure 26, it can be seen that the pore size distribution from the simulation is closer to Wood's metal image analysis, than to mercury intrusion porosimetry.

6 Conclusions

In this paper, the three-dimensional simulated microstructure of cement pastes were visualized and analyzed. Some general conclusions can be drawn:

1. A serial section algorithm with an overlapping criterion was applied to analyze the simulated microstructure. The geometrical parameters, including the internal surface area, the hydraulic radius and the total capillary porosity, can be obtained. The topological properties, including the connectivity, in terms of genus number, can also be determined with this algorithm. The pore size distribution was computed by packing pore spheres in the free space.
2. The simulation results by the HYMOSTRUC3D showed that the microstructural properties of the hardening cement paste strongly depend on the w/c and on the cement particle size distribution. The pore size distribution covered a wide range of the samples with a high w/c and for coarser cement. Smaller pores exist in the samples with lower w/c and finer cement, meaning that a more complex fluid channel is formed. For the same w/c, cement with finer particles had a lower percolation threshold than coarser cements.
3. The percolation theory was applied to explain the evolution of the phases in cement paste. It was found that the connectivity is strongly influenced by the digital resolution used in the calculation.

4. The simulated pore size distributions with HYMOSTRUC3D were compared with the experiments of SEM and mercury intrusion porosity test. It was found that the simulated pore sizes were one order of magnitude greater than those measured by MIP tests, while the shape of the pore size distribution curve was quite similar to that obtained by processing of SEM images of the cement paste.

7 Acknowledgement

The research was financially supported by the Dutch Technology Foundation (STW), which is gratefully acknowledged.

Reference

[1] Van Breugel, K. (1991) Simulation of hydration and formation of structure in hardening cement-based materials, PhD thesis, Delft University of Technology, Delft.

[2] Laszlo, M. (1995) Computational Geometry and Computer Graphics in C++, Prentice Hall.

[3] Serra, J. Image analysis and mathematical morphology, Academic Press, London, 1982.

[4] Dullien, F.A.L. (1992) *Porous Media: Fluid Transport and Pore Structure*, Second Edition, Academic Press, San Diego.

[5] Dullien, F.A.L. (1991) 'Characterization of porous media-pore level', Transport in Porous Media, vol. 6, pp. 581-60.

[6] MacDonald, I.F., Kaufman, P. and Dullien, F.A.L. (1986a) 'Quantitative image analysis of finite porous media, I. Development of genus and pore map software', Journal of Microscopy, vol. 144 pp. 277-296.

[7] MacDonald, I.F., Kaufman, P. and Dullien, F.A.L. (1986b) 'Quantitative image analysis of finite porous media, ii. Specific genus of cubic lattice models and Berea sandstone', Journal of Microscopy, vol. 144 pp. 297-316.

[8] Lymberopoulos, D.P. and Payatakes, A.C. (1992) Derivation of topological, geometrical, and correlation properties of porous media from pore-chart analysis of serial section data, Journal of Colloid Interface Science, vol. 150 (1) pp. 61-80.

[9] Liang, Z., Ioannidis, M.A. and Chatzis, I. (2000) '3D pore structure based on skeletonization', Chemical Engineering Science, vol. 55 pp. 5247-5262.

[10] Bekri, S., Xu, K., Yousefian, F., Adler, P.M., Thovert, J.-F., Muller, J., Iden, K., Psyllos, A., Stubos, A.K. and Ioannidis, M. A. (2000) 'Pore geometry and transport properties in north sea chalk', Journal of Petroleum Science and Engineering, vol. 25 pp. 107-134.

[11] Jiang, S.P., Detriche, Ch. and Grandet, J. (1992) 'Relationships between mechanical properties of mortars and the hydraulic radius of their pores', 9th International Congress on the Chemistry of Cement, New Delhi, India, vol.5 pp.191-195.

[12] Powers, T.C. and Brownyard, T.L. (1947) 'Studies of the physical properties of hardened portland cement paste', Journal of the American Concrete Institute, vol. 18 (7).

[13] Ye, G. (2003) Experimental study and numerical simulation of the development of the microstructure and permeability of cementitious materials, PhD thesis, Delft University of Technology, Delft.

[14] Bentz, D.P. and Garboczi, E.J. (1991) 'Percolation of phases in a three-dimensional cement paste microstructural model', Cement and Concrete Research, vol. 21 pp. 324-344.

[15] Boumiz, B., Vernet, C. and Cohen, F.T. (1996) 'Mechanical Properties of Cement Pastes and Mortars', Advanced Cement-based Materials, vol. 3 pp. 94-106.

[16] Reinhardt, H.W. and Grosse, C.U. and Herb, A.T. (2000) 'Ultrasonic monitoring of setting and hardening of cement mortar - A new device', Materials and structures/Matériaux et Constructures vol. 33 pp. 581-583.

[17] Rapoport, J., Popovics, J.S., Subramaniam, K.V. and Shah, S.P., (1997) 'The use of ultrasound to monitor the stiffening process of Portland cement concrete with admixtures', ACI Mater. J., vol. 6 pp. 675-683.

[18] Garboczi, E.J. and Bentz, D.P. (2001) 'The effect of statistical fluctuation, finite size error, and digital resolution on the phase percolation and transport properties of the NIST cement hydration model', Cement and Concrete Research, vol. 31 (11) pp. 1501-1514.

[19] Navi, P. and Pignat, C. (1996) 'Simulation of cement hydration and the connectivity of the capillary pore space', Advanced Cement Based Material, vol. 4 pp. 58-67.

[20] Elam, W.T., Kerstein, A.R. and Rehr, J.J. (1984) 'Critical properties of the void percolation problem for spheres', Physical Reviewer Letters, vol.52 pp. 1516-1519.

[21] Lange, D.A., Jennings, H.M. and Shah, S.P. (1994) 'Image analysis techniques for characterization of pore structure of cement-based materials' Cement and Concrete Research, vol. 24 (5) pp.841-853.

[22] Willis, K.L., Abell, A.B. and Lange, D.A. (1998) 'Image-based characterization of cement pore structure using wood's metal intrusion', Cement and Concrete Research, vol. 28 (12) pp. 1695-1705.

[23] Diamond, S. (2000) 'Mercury porosimetry: an inappropriate method for the measurement of pore size distributions in cement-based materials', Cement and Concrete Research, vol. 30 (10) pp. 1517-1525.